Coupling two and one-dimensional unsteady Euler equations through a thin interface

Jean-Marc Hérard, Olivier Hurisse

COUPLING TWO AND ONE DIMENSIONAL UNSTEADY EULER EQUATIONS THROUGH A THIN INTERFACE

Jean-Marc Hérard[1,2,*], Olivier Hurisse[1,2]

[1] Électricité de France, Division Recherche et Développement,
Département Mécanique des Fluides, Energies et Environnement,
6 quai Watier, 78401 Chatou cedex, FRANCE
jean-marc.herard@edf.fr, olivier.hurisse@edf.fr

[2] Université de Provence, Centre de Mathématiques et d'Informatique,
Laboratoire d'Analyse, Topologie et Probabilités - UMR 6632,
39 rue Joliot Curie, 13453 Marseille cedex 13, FRANCE
hurisse@cmi.univ-mrs.fr

Abstract

We present herein a method for the numerical coupling of one and two-dimensional Euler isentropic models through a thin interface. The basic approach is connected with recent works by E. Godlewski, A.Y. Leroux and P.A. Raviart. It requires introducing an interface model, and solving the associated Riemann problem at the interface between codes. Numerical results confirm both the stability and the fair accuracy of the admissible non-conservative approach, which is also compared with an admissible conservative approach and a reference two-dimensional solution. The extension to the full Euler set of equations is also briefly discussed.

1 Introduction

The problem of the coupling of distinct models described by sets of PDE is a topic which has become of growing interest over the past few years. Actually, it may first occur in the framework of the modelling of two-phase flow in porous media. In that case, one has to face conservation laws with discontinuous flux functions, and one of the main difficulties consists in proving the existence and uniqueness of a physically relevant solution. One may for instance refer to [6] , [7], [24] and references therein. It also naturally arises when focusing on industrial projects where

*Corresponding author

computational facilities require the use of different models in order to describe parts of a whole concept. This happens for instance when one aims at computing the flow around a whole plane, or alternatively the flow in a gas turbine engine (decomposed in combustion chamber and turbine section, see [23], [21], [22] for instance). It also immediately occurs when turning to the predictive computations of the flow in the primary coolant circuit of a pressurized water reactor, in a nuclear power plant (see [10]). In the latter case, one sometimes needs to account for the flow in the reactor, in pipes and in the steam generator. Actually, one may apply for a 1D code to deal with the pipe, and a 3D code to predict the flow in the reactor. In addition, the 1D code may include schemes which provide approximations of a six-equation two-fluid model, whereas the 3D code deals with an homogeneous two phase flow model such as HEM (homogeneous equilibrium model) or HRM (homogeneous relaxation model). The problem of the coupling in such a situation is obviously a tedious and ambitious topic, and it also suggests as a prerequisite that one knows how to couple simpler situations such as the following for instance :

(i) the coupling of two distinct models in a one dimensional framework ;

(ii) the coupling of the homogeneous equilibrium model in a 1D pipe and a three dimensional medium.

We will focus in this paper on the problem (ii). We refer for instance to [4], [2], and [20], which try to address the first problem (i) while focusing on HEM and HRM models, and also mention [3], [5] that tackle the coupling of Euler equations with distinct equations of state in each code. We insist that we only want to provide suitable information to be exchanged through the interface, and a (of course stable) numerical way to implement it. Both codes on each side should not be modified by the new procedure, except that boundary conditions may be different from what they were before coupling.

Quite recently, a few authors have suggested some new ideas to couple subsets of PDE. A first approach has been suggested by A.Y. Leroux and co-authors (see [17] for instance). It has been essentially applied to cope with the shallow water equations with topography. The main idea in the latter approach is to include a stationary constraint in the set of PDE with an augmented state variable, and then to solve the exact Riemann problem at the "stationary" interface. The resulting scheme has been proved to be an efficient way to cope with steady state situations ([12]). We emphasize that we will apply for similar ideas in our approach. A second way to tackle with this problem has emerged recently too, and is detailed in [13], [15] in a specific situation. In fact, it may be seen as an extension of ideas in the paper [1], which is roughly grounded on the following idea: initial conditions are used twice to compute two different fluxes at the interface between cells ; the first one is obtained solving the exact Riemann problem with the *left* set of PDE, whereas the second one corresponds to the *right* set of PDE. We refer for instance to [4] for more details.

The present paper is organized as follows. We first briefly recall in section 2 the basic sets of equations on each side of the interface between codes. In the beginning of section 3, we exhibit a natural constraint which obviously arises. We then detail a natural interface model and two distinct interface models which may be used to exchange information through the interface for unsteady predictions. The associated left and right fluxes will be detailed. Section 4 is devoted to the presentation of schemes that will be used, and of numerical results. Computational results involving shock waves with great inhomogeneities of transverse velocities between both medium will be discussed, and this will be achieved on the basis of the L^1 norm of the error. Actually, results obtained when computing unsteady solutions traveling from a 2D tank to the 1D pipe will

be compared with those obtained while using the 2D code over the whole domain. The comparison will include :
(a) the effect of mesh refinement;
(b) the sensitivity with respect to the EOS;
(c) the influence of the location of the interface between codes on numerical results;
(d) the influence of the interface model.
For further details, the reader is referred to [20]. The extension of these ideas to the framework of non-isentropic Euler equations is also briefly examined in an appendix.

This work is a contribution to the NEPTUNE joint project, and is part of recent investigations which aim at improving the numerical interfacial coupling of two-phase flow codes (see [18], [19], [20] among others).

2 Models

2.1 Codes to be coupled

For the sake of simplicity we consider the isentropic Euler model. We want to couple the one-dimensional isentropic Euler system to the two-dimensional isentropic Euler system through a thin interface. Without loss of generality we consider that the interface is along the y-axis.

On the left side of the interface we consider the one-dimensional isentropic Euler system $(1D)$: ù

$$\frac{\partial W_1}{\partial t} + \frac{\partial F(W_1)}{\partial x} = 0 \tag{1}$$

with:

$$\begin{cases} W_1 = (\rho, \rho u) \\ F(W_1) = (\rho u, \rho u^2 + P(\rho)) \end{cases}$$

where u, ρ and P respectively stand for the velocity, the density and the pressure, with $P'(\rho) > 0$. These variables only depend on the time t and the space dimension x, $W_1 = W_1(x,t)$.

On the right side of the interface we consider the two-dimensional isentropic Euler system $(2D)$:

$$\frac{\partial W_2}{\partial t} + \frac{\partial G_1(W_2)}{\partial x} + \frac{\partial G_2(W_2)}{\partial y} = 0 \tag{2}$$

with:

$$\begin{cases} W_2 = (\rho, \rho u, \rho v) \\ G_1(W_2) = (\rho u, \rho u^2 + P(\rho), \rho uv) \\ G_2(W_2) = (\rho v, \rho uv, \rho v^2 + P(\rho)) \end{cases}$$

Here u denotes the component of the velocity along the x-axis and v the component of the velocity along the y-axis. Here all the variables depend on time t and on two space variables x and y, $W_2 = W_2(x,y,t)$.

2.2 The one-dimensional model

We recall herein some well-known properties of the conservative system (1). This will be useful in section 4.

2.2.1 Eigenstructure

In terms of the variable $Y = (\rho, u)$, and setting $c^2 = P'(\rho)$, (1) writes in non-conservative form:

$$\frac{\partial Y}{\partial t} + A(Y)\frac{\partial Y}{\partial x} = 0$$

where the 2×2 convection matrix A is:

$$A(Y) = \begin{pmatrix} u & \rho \\ \frac{c^2}{\rho} & u \end{pmatrix}$$

The eigenvalues and the right eigenvectors of the matrix A are:

$$\lambda_1 = u - c, \quad r_1^\top = (\rho, -c)$$

$$\lambda_2 = u + c, \quad r_2^\top = (\rho, c)$$

Thus, until vacuum occurs, eigenvalues are real and distinct ; the system is unconditionally hyperbolic since the two eigenvectors span the plane $\mathbb{R}^2$. Moreover both fields are genuinely non-linear.

2.2.2 Entropy pair

One may easily check that an entropy pair $(\eta(W_1), F_\eta(W_1))$ is:

$$\begin{array}{l} \eta(W_1) = \frac{\rho u^2}{2} + \rho\psi(\rho) \\ F_\eta(W_1) = (\eta(W_1) + P(\rho))u \end{array}$$

with $\psi(\rho) = \int_0^\rho \frac{P(a)}{a^2} da$. Moreover η is strictly convex with respect to W_1. Hence the Riemann problem associated with (1) has a unique entropy consistent solution composed of constant states separated by shocks and rarefaction waves, with no vacuum occurrence, provided that the initial data agrees with the condition:

$$u_R - u_L < g(\rho_L) + g(\rho_R)$$

where: $g'(\rho) = \frac{c(\rho)}{\rho}$ -see [25] and [14] -.

2.2.3 Solution for the Riemann problem

We describe herein the main features of the solution of the Riemann problem.

We set (u_L, ρ_L) and (u_R, ρ_R) the left and right state for the Riemann problem associated with system (1). The right and left pressure for initial state are respectively $P_R = P(\rho_R)$ and $P_L = P(\rho_L)$. We set (u^*, ρ^*) to be the intermediate state between the two waves and we set $P^* = P(\rho^*)$.

- Trough the 1-wave, we get:

  $$u^* - u_L = h_L(P_L, P^*)$$

  If $P_L < P^*$, the 1-wave is a shock wave:

  $$h_L(P_L, P^*) = -\sqrt{\frac{(P^* - P_L)(\rho^* - \rho_L)}{\rho_L \rho^*}}$$

  otherwise the 1-wave is a rarefaction wave:

  $$h_L(P_L, P^*) = g(\rho_L) - g(\rho^*)$$

- Trough the 2-wave, we get:

  $$u^* - u_R = h_R(P_R, P^*)$$

  If $P_R < P^*$, the 2-wave is a shock wave:

  $$h_R(P_R, P^*) = \sqrt{\frac{(P^* - P_R)(\rho^* - \rho_R)}{\rho_R \rho^*}}$$

  otherwise the 2-wave this is a rarefaction wave:

  $$h_R(P_R, P^*) = g(\rho^*) - g(\rho_R)$$

2.3 The two-dimensional model

We can write the system (2) in a non-conservative form using the variable $Z^\top = (\rho, u, v)$:

$$\frac{\partial Z}{\partial t} + B_x(Z)\frac{\partial Z}{\partial x} + B_y(Z)\frac{\partial Z}{\partial y} = 0$$

with the following 3×3 matrix B_x and B_y:

$$B_x(Z) = \begin{pmatrix} u & \rho & 0 \\ \frac{c^2}{\rho} & u & 0 \\ 0 & 0 & u \end{pmatrix}$$

$$B_y(Z) = \begin{pmatrix} v & 0 & \rho \\ 0 & v & 0 \\ \frac{c^2}{\rho} & 0 & v \end{pmatrix}$$

For any $(w_1, w_2) \in \mathbb{R}^2 - \{(0,0)\}$ with $w_1^2 + w_2^2 = 1$, we set $C(Z, w) = w_1 B_x(Z) + w_2 B_y(Z)$. The system (2) is hyperbolic if for any (w_1, w_2) and for any $Z \in \Omega$, the matrix $C(Z, w)$ has three real eigenvalues and three independent eigenvectors. It is easy to verify that the eigenvalues of $C(Z, w)$ are real:

$$\lambda_1 = (w_1 u + w_2 v)$$

$$\lambda_2 = (w_1 u + w_2 v) - c\sqrt{w_1^2 + w_2^2}$$

$$\lambda_2 = (w_1 u + w_2 v) + c\sqrt{w_1^2 + w_2^2}$$

The corresponding eigenvectors are clearly independent until vacuum occurs:

$$r_1^\top = (0, w_2, w_1)$$

$$r_2^\top = (\rho, \tfrac{w_1 c}{\sqrt{w_1^2+w_2^2}}, \tfrac{w_2 c}{\sqrt{w_1^2+w_2^2}})$$

$$r_3^\top = (\rho, -\tfrac{w_1 c}{\sqrt{w_1^2+w_2^2}}, -\tfrac{w_2 c}{\sqrt{w_1^2+w_2^2}})$$

3 The interface model

Obviously, a two-dimensional code (based on a two-dimensional system) applied on a "one-dimensional" domain does not behave as a one-dimensional code (based on a one-dimensional system) on the same domain. Nonetheless we want to look for a condition for a 2D code to behave as a 1D code.

3.1 A necessary condition: NSC

Let us first define a test problem resumed on the figure (1). A pipe ($x < 0$) is connected to a tank ($x > 0$) at $x = 0$ (see figure (1)). Suppose that the domain ($x < 0$) is discretized by a raw of rectangular cells with volume $\Delta x \times h$. We note ϕ^{God} the value of the field ϕ given by a Godunov method and the subscripts H_i, B_i, D_i and G_i denote respectively the upper, lower, right and left side of the cell i.

Focusing on the transverse component of the momentum, ρv, we write a Godunov [16] scheme in the domain $x < 0$ as:

$$\begin{aligned} & h\Delta x((\rho v)_i^{n+1} - (\rho v)_i^n) \\ & +\Delta t\Delta x \left[(\rho v^2 + P)_{H_i}^{God} - (\rho v^2 + P)_{B_i}^{God}\right] \\ & +h\Delta t \left[(\rho uv)_{D_i}^{God} - (\rho uv)_{G_i}^{God}\right] = 0 \end{aligned} \tag{3}$$

Let us set, for all cells in the domain $x < 0$, $v_i^n = 0$. Using wall condition [8] as a boundary condition, defining $\overrightarrow{N_{H_i}}$ ($\overrightarrow{N_{B_i}}$ respectively) as the unit outward normal vector on the top wall (bottom wall respectively), the pressure on the boundary of the left domain writes:

$$P_{H_i}^{God} = P^{God}(W_i^n, \hat{W}_{H_i}^n, \overrightarrow{N_{H_i}})$$

$$P_{B_i}^{God} = P^{God}(W_i^n, \hat{W}_{B_i}^n, \overrightarrow{N_{B_i}})$$

where $\hat{W}_{H_i}^n = \hat{W}_{B_i}^n = \hat{W}_i^n = (\rho_i^n, (\rho u)_i^n, -(\rho v)_i^n)$ stands for the mirror state of W_i^n.

Then the above initial condition on the velocity implies that for all cells in the domain $x < 0$:

$$P_{H_i}^{God} = P_i^n = P_{B_i}^{God}$$

$$v_{H_i}^{God} = v_{B_i}^{God} = v_{G_i}^{God} = 0$$

and if we are in the domain $x < -\Delta x$

$$v_{D_i}^{God} = 0$$

So that if we assume that vacuum does not appear ($\rho_i^n > 0$) in these cells, the preceding equation (3) provides $v_i^{n+1} = 0$ for all cells except for the cell i_0 (see figure (1)) which has its right side on the interface $x = 0$. Indeed nothing ensures that $v_{D_{i0}}^{God} = 0$ for this particular cell.

This gives us a necessary and sufficient condition (NSC) for a scheme to fit to pure one-dimensional simulation in the left domain.

Definition:
We will say that the coupling boundary conditions will be admissible if the ρv component of the flux at the interface $x = 0^-$ is null, that means:

$$(\text{NSC}) : (\rho uv)^- = 0$$

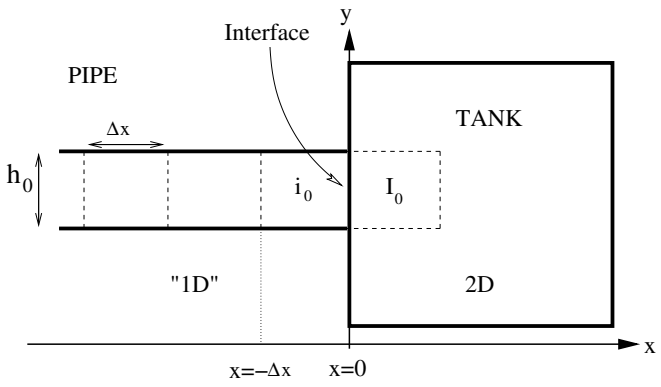

Figure 1: The test problem

We now investigate some possible interface models to couple the one-dimensional domain $x < 0$ to the two-dimensional domain $x > 0$. Interface models are introduced to allow the computation of Godunov fluxes through the vertical interface $x = 0^{\pm}$. In practice, we recall that they are only used to compute $(\rho uv)(x/t = 0^-)$ and $(\rho uv)(x/t = 0^+)$, as sketched in figure (2).

In the left domain we consider the system (1) extended with the variable v and one aim of an admissible interface model is to maintain $v = 0$ in this domain by fullfilling the (NSC). An admissible interface model must also give the model (1) on the left of the interface and the projection on the normal of the model (2) on the right.

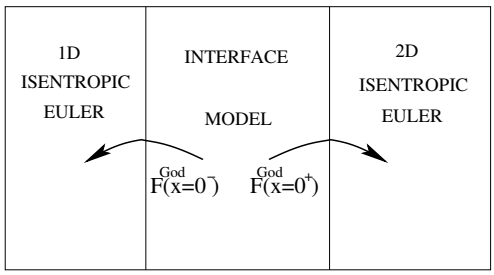

Figure 2: The interface model

We successively consider :

- A natural model at the interface
- A non conservative admissible interface model

- A conservative admissible interface model

3.2 A natural model at the interface

An *a priori* obvious candidate as an interface model immediately arises considering the projection on a vertical interface of the model (2):

$$\frac{\partial \rho}{\partial t} + \frac{\partial \rho u}{\partial x} = 0 \tag{4}$$

$$\frac{\partial \rho u}{\partial t} + \frac{\partial \rho u^2 + P}{\partial x} = 0 \tag{5}$$

$$\frac{\partial \rho v}{\partial t} + \frac{\partial \rho u v}{\partial x} = 0 \tag{6}$$

We briefly recall now the structure of the Riemann problem associated with ((4)-(6)) at the interface $x = 0$ with left state,

$$W_2^L = (\rho_L, \rho_L u_L, \rho_L v_L = 0)^\top$$

and right state,

$$W_2^R = (\rho_R, \rho_R u_R, \rho_R v_R)^\top$$

to determine the Godunov flux at $x = 0^\pm$.

In terms of the variable $Y = (\rho, u, v)^\top$, the eigenvalues and the right eigenvectors of the system (4)-(6) are:

$$\lambda_1 = u - c, \quad r_1^\top = (\rho, -c, 0)$$

$$\lambda_2 = u, \quad r_2^\top = (0, 0, 1)$$

$$\lambda_3 = u + c, \quad r_3^\top = (\rho, c, 0)$$

The subsystem ((4),(5)) has been briefly described above. We set u^* and ρ^* the intermediate states for u and ρ between the two waves λ_1 and λ_3 as described below for the system (1). We set v_1^* (respectively v_2^*) the intermediate state for v between λ_1 and λ_2 (respectively between λ_2 and λ_3) (see figure (3))

Focusing on the variable v, we observe that through the first and third waves $[v] = 0$ and that v is a Riemann invariant of the first and third field. Hence the solution for v is, $v_1^* = v_L$ and $v_2^* = v_R$, and so:

$$v(x/t; W_2^L, W_2^R) = \begin{cases} v_L = 0, \text{ if } x/t < u^* \\ \\ v_R, \text{ if } x/t > u^* \end{cases}$$

We assume from now that the 2-wave does not coincide with $x/t = 0$. As a consequence the ρv-component of the Godunov flux at $x/t = 0$ is:

$$(\rho u v)(x/t = 0; W_2^L, W_2^R) = \begin{cases} (\rho u)(x/t = 0) v_L = 0, \text{ if } u^* > 0 \\ \\ (\rho u)(x/t = 0) v_R, \text{ if } u^* < 0 \end{cases}$$

Of course, in general $v_R \neq 0$, so that $F^{God}(x = 0^-)$ is not always null if $u^* < 0$. Thus this interface model does not respect the (NSC), which results in the fact that v will not remain zero in the

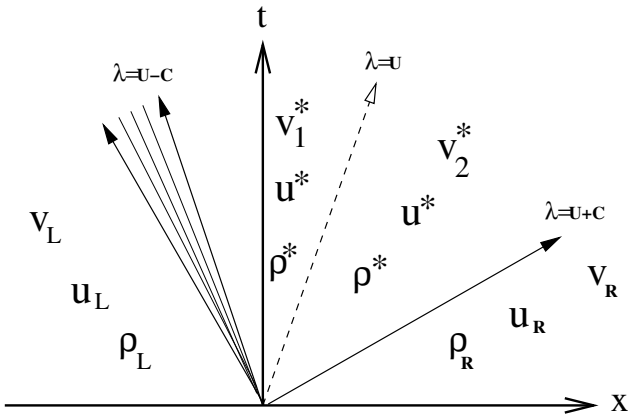

Figure 3: Intermediate states for u, ρ and v

one-dimensional domain.

It must thus be rejected if one aims at computing the solutions in the 1D computational domain with a 2D algorithm and a raw of cells.

3.3 A non conservative admissible interface model

Following [17] we introduce here a new variable which distinguishes the two domains and does not depend on time t,

$$z(x,y,t) = \begin{cases} 0 \text{ if } x < 0 \\ \\ 1 \text{ if } x > 0 \end{cases}$$

We now consider the following interface model:

$$\frac{\partial z}{\partial t} = 0 \tag{7}$$

$$\frac{\partial \rho}{\partial t} + \frac{\partial \rho u}{\partial x} = 0 \tag{8}$$

$$\frac{\partial \rho u}{\partial t} + \frac{\partial \rho u^2 + P}{\partial x} = 0 \tag{9}$$

$$\frac{\partial v}{\partial t} + zu\frac{\partial v}{\partial x} = 0 \tag{10}$$

with initial condition $v(x,y,t=0) = 0$ for all $x < 0$. We note that (10) enables to retrieve

$$\frac{\partial v}{\partial t} = 0$$

on the left hand side and

$$\frac{\partial v}{\partial t} + u\frac{\partial v}{\partial x} = 0$$

on the right hand side -which (thanks to (8)), is equivalent to (6)-.

Using the set of variables $Y^\top = (z, \rho, u, v)$ the eigenvalues and the right eigenvectors of the system (7)-(10) are:

$$\lambda_1 = 0, \quad r_1^\top = (1, 0, 0, 0)$$

$$\lambda_2 = u - c, \quad r_2^\top = (0, \rho, -c, 0)$$

$$\lambda_3 = u + c, \quad r_3^\top = (0, \rho, c, 0)$$

$$\lambda_4 = zu, \quad r_4^\top = (0, 0, 0, 1)$$

The fields 1 and 4 are linearly degenerated while the fields 2 and 3 are genuinely non-linear.

Moreover we can write the Rankine-Hugoniot relations for a shock with *non-zero* speed σ :

$$\begin{cases} -\sigma[z] = 0 \\ -\sigma[\rho] + [\rho u] = 0 \\ -\sigma[\rho u] + [\rho u^2 + P] = 0 \\ \begin{cases} -\sigma[v] = 0 \text{ if } \sigma < 0 \\ -\sigma[\rho v] + [\rho u v] = 0 \text{ if } \sigma > 0 \end{cases} \end{cases}$$

For $\sigma = 0$, one has $[\rho u] = [\rho u^2 + P] = 0$, and z may jump. However, Rankine-Hugoniot conditions on the tranverse component are undefined . In that case, the 1-field would coincide with a genuinely non linear field.

The Rankine-Hugoniot relations imply that in a shock $[z] = 0$ if and only if $\sigma \neq 0$, that is in the 2-shock, 3-shock and 4-waves. For $\sigma > 0$, the above system provides the equation :

$$\overline{\rho(u - \sigma)}[v] = 0 \tag{11}$$

Thus, if $\sigma > 0$, $[v] = 0$ in the 2-shock or 3-shock waves since $\sigma \neq \overline{\rho u}/\overline{\rho}$. If we focus on the 4-wave (contact wave) propagating in the region $x > 0$, we retrieve the trivial solution $\sigma = \overline{u}$ which provides no constraint for v. On the other side, if $\sigma < 0$, the relation $-\sigma[v] = 0$ also implies that $[v] = 0$.

The subset ((8),(9)) involves u and ρ and is the classical one dimensional isentropic Euler model which gives the solution (u^*, ρ^*) (see figure (3) and section 2.2.3). The Riemann invariants of the system are:

$$IR_1 = \{\rho, u, v\}$$

$$IR_2 = \{z, v, u + g(\rho)\}$$

$$IR_3 = \{z, v, u - g(\rho)\}$$

$$IR_4 = \{z, \rho, u\}$$

Since the first field is linearly degenerated and since z is preserved through the 2-wave, the 3-wave and the 4-wave:

$$z(x, y, t) = \begin{cases} z_R = 1 & \text{if } x > 0 \\ z_L = 0 & \text{if } x < 0 \end{cases}$$

Since v is preserved through the 1-wave, the 2-wave and the 3-wave:

$$v(x/t = 0^-) = v_L = 0$$

$$v(x/t=0^+) = \left\{ \begin{array}{l} v^- = v_L \ \text{ if } \ \lambda_4 > 0 \\ v_R \ \text{ if } \ \lambda_4 \leq 0 \end{array} \right.$$

We emphasize that the 4-contact wave cannot travel to the left domain because $z(x<0,y,t)=0$. This leads to the numerical flux on the ρv-component :

- <u>if $u^* > 0$:</u>

$$(\rho uv)(x/t=0^-) = 0$$

$$(\rho uv)(x/t=0^+) = 0$$

- <u>if $u^* < 0$:</u>

$$(\rho uv)(x/t=0^-) = 0$$

$$(\rho uv)(x/t=0^+) = (\rho u)(x/t=0)v_R$$

Since $(\rho uv)(x/t=0^-)$ is always null, this model respects the (NSC).

Remark. *An important point to be quoted is that we obtain the same discrete fluxes using the Godlewski-Raviart method [13],[15] with fluxes:*

$$f_L = \begin{pmatrix} \rho u \\ \rho u^2 + P \\ 0 \end{pmatrix} \text{ and } f_R = \begin{pmatrix} \rho u \\ \rho u^2 + P \\ \rho uv \end{pmatrix}$$

Remark. *We check now the continuity of $(\rho uv)(x/t=0^{\pm})$ with respect to u^* at $u^*=0$. This is important for the stability of cases which involve states at rest around the interface. Of course, we always have $(\rho uv)(x/t=0^-)=0$ whatever u^* is. Hence:*

$$\lim_{u^* \to 0^-} (\rho uv)(x/t=0^-) = 0 = \lim_{u^* \to 0^+} (\rho uv)(x/t=0^-)$$

We focus now on $(\rho uv)(x/t=0^+)$. First of all, we have:

$$\lim_{u^* \to 0^+} (\rho uv)(x/t=0^+) = 0$$

We eventually want to prove that $\lim_{u^* \to 0^-} (\rho uv)(x/t=0^+) = 0$. For that purpose we need to introduce a new variable q and its governing equation:

$$\frac{\partial \rho q}{\partial t} + \frac{\partial \rho uq}{\partial x} = 0$$

The eigenvalue associated with this new linearly degenerated field is $\lambda_5 = u$ which, unlike $\lambda_4 = zu$, can be negative. *This will enable to find the limit of $(\rho uv)(x/t=0^+)$ when u^* tends towards 0^-. This new variable q and its governing equation do not change the structure of the solution for z, ρ, u and v. Since u only varies through the 2-wave and the 3-wave, and since $\lambda_5 = u^*$, we have:*

$$\lim_{\lambda_5 \to 0^-} u(x/t=0) = \lim_{\lambda_5 \to 0^-} u(x/t=0^-) = \lim_{\lambda_5 \to 0^-} u^* = 0$$

hence,

$$\lim_{u^* \to 0^-} (\rho uv)(x/t=0^+) = 0$$

3.4 A conservative admissible model at the interface

We still use:

$$z = \begin{cases} 0 \text{ if } x < 0 \\ 1 \text{ if } x > 0 \end{cases}$$

We consider the conservative interface model:

$$\frac{\partial z}{\partial t} = 0 \tag{12}$$

$$\frac{\partial \rho}{\partial t} + \frac{\partial \rho u}{\partial x} = 0 \tag{13}$$

$$\frac{\partial \rho u}{\partial t} + \frac{\partial \rho u^2 + P}{\partial x} = 0 \tag{14}$$

$$\frac{\partial \rho v}{\partial t} + \frac{\partial z \rho u v}{\partial x} = 0 \tag{15}$$

In the right region $(x/t > 0)$ one recovers the projection of the model (2). For $(x/t < 0)$, (14) reads $\frac{\partial \rho v}{\partial t} = 0$, and can be integrated, which provides $\rho v(x < 0, t > 0) = 0$ since $v(x < 0, t = 0) = 0$. One thus clearly retrieves the onedimensional model $v(x < 0, t > 0) = 0$ for positive densities (vacuum occurence is beyond the scope of our approach).

In terms of the non-conservative variables $Y^\top = (z, \rho, u, \rho v)$, the eigenvalues an eigenvectors of the jacobian matrix associated to the system (12)-(15) are:

$$\lambda_1 = 0, \quad r_1^\top = (z, 0, 0, -\rho v)$$

$$\lambda_2 = u - c, \quad r_2^\top = (0, \rho, -c, \tfrac{-\rho v c z}{(u-c)-uz})$$

$$\lambda_3 = u + c, \quad r_3^\top = (0, \rho, c, \tfrac{\rho v c z}{(u+c)-uz})$$

$$\lambda_4 = zu, \quad r_4^\top = (0, 0, 0, 1)$$

The first and fourth fields are linearly degenerated while the second and third fields are genuinely non-linear. Jump conditions are uniquely defined.

An important point to be quoted is that the subset of equations (13)-(14) does not depend on z or v. Thus the solution of a Riemann problem for (12)-(15) will give for the pair (ρ, u) the same solution as the Riemann problem for the sole equations (13)-(14) when considering the same initial condition for ρ and u (see section 2.2.3). Hence, we focus now on the transverse component of the flux.

We first consider the Rankine-Hugoniot relation through the first wave. We have:

$$[\rho u z v] = 0 \quad \text{and} \quad [\rho u] = 0$$

which implies:

$$[zv] = 0 \tag{16}$$

(unless $(\rho u)(x = 0, t > 0) = 0$, which does not modify the conclusions). The only Riemann problems that are relevant for our purpose are those for which right and left states comply with:

$$z_L = 0 \quad \text{and} \quad z_R = 1 \quad \text{and} v_L = 0$$

With this initial condition, (12) enables to retrieve $z(x < 0, t > 0) = 0$ and $z(x > 0, t > 0) = 1$. Assuming that no resonnance phenomenon occurs, the equation (16) implies that the transverse velocity at $x/t = 0^+$ is:

$$v^+ = 0$$

Hence the transverse flux at $x/t = 0^+$ for such Riemann problems is:

$$(\rho uzv)^+ = (\rho uv)^+ = 0 \tag{17}$$

We may retrieve this simply considering :$[\rho uzv] = 0$, which gives $(\rho uzv)^+ - (\rho uzv)^- = 0$ or $(\rho uzv)^+ = (\rho uv)^+ = 0$. We do not need to assume that $v^- = 0$ to obtain the relation (17).

Since $z^- = 0$, we have no information on the "transverse flux" (ρuv) at $x/t = 0^-$ when focusing on the first wave. We can only conclude that $(\rho uzv)^- = 0$. In order to revover relevant information, we need to consider the half plane $x/t < 0$. The only waves which can develop in the domain $x/t < 0$ are the two genuinely non-linear waves associated with λ_2 and λ_3. Since $z(x/t < 0) = 0$, the equation (15) reads:

$$\frac{\partial \rho v}{\partial t} = 0, \quad \forall (x/t) < 0$$

Hence, if we assume that the left transverse velocity in the initial condition of the Riemann problem is $v_L = 0$, and thus that $\rho_L v_L = 0$, we obtain $(\rho v)^- = 0$. We can conclude that the transverse flux at $x/t = 0^-$ is:

$$(\rho uv)^- = 0 \tag{18}$$

This conservative interface model thus respects the (NSC) condition in the frame of a Riemann problem with correct initial condition $v_L = 0$.

4 Numerical schemes and results

All methods described herein rely on the Finite Volume method (see [9]). Instead of using the exact Godunov scheme, we apply herein for the approximate Godunov scheme VFRoe-ncv introduced in [8], using the non conservative variable $Y^\top = (\rho, u, v)$. We restrict here to the so-called "first-order" scheme. Wall boundary conditions are accounted for by using the standard mirror approach. ([8] and [14]).

4.1 The computational domain

4.1.1 The coarse mesh

The above method will be tested on a domain composed of a pipe connected to the middle of the left side ($x = 0$) of a squared tank. The pipe is 2 unit long and $h_0 = \frac{2}{21}$ unit high; the sides of the tank are 2 unit long. The initial mesh (see fig:(4)) contains 21×21 regular square cells in the tank and 21 cells in the pipe. Hence all the cells of this initial mesh are squares of the same size $h_0 = \frac{2}{21}$.

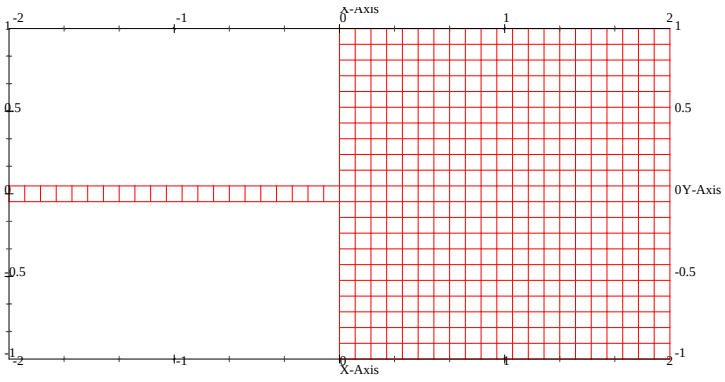

Figure 4: The coarse mesh

4.1.2 Position of the interface

Two different positions for the interface $x_{interf} = \{0, -5h_0\}$, where h_0 is the diameter of the pipe, are used to define the boundary between one- and two-dimensional domains on the initial mesh (see fig:(5)). That is, the domain on the left of $x = x_{interf}$ is the one-dimensional domain and the domain on the right is the two-dimensional domain.

4.1.3 Mesh refinement

We use three levels of refinement. The cells of the two-dimensional domain are respectively cut into 2, 4 and 8 in each direction. The one-dimensional domain cells are respectively cut into 2, 4 and 8 in the x direction (see fig:(5)). The last cell on the right side of the one-dimensional domain thus

has 4, 5, 7 and 11 edges, depending on the mesh level refinement. The finest grid approximately contains 30000 nodes.

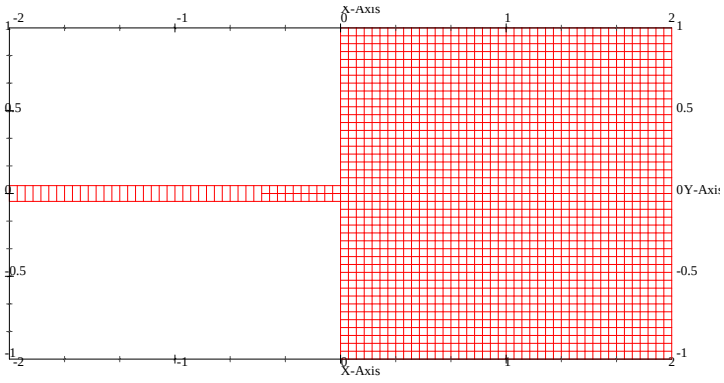

Figure 5: Example of mesh for $x_{interf} = -5h_0$ and for the first level of refinement

4.2 Initial conditions and EOS parameters

We consider herein a Riemann problem derived from the shock tube experiment. As initial conditions, we set ρu and ρv equal to zero on the whole domain and for the density we set:

$$\rho(x, y; t = 0) = \begin{cases} \rho_l & \text{if } y > x - 0.15 \\ \rho_r & \text{else.} \end{cases}$$

These initial conditions seem to be the worst configuration to test the coupling methods. Actually, we intend to maximize $(\rho uv)^+$, in order to track possible deficiencies. The most tedious situation appears when the fluid flows from the tank into the pipe with "high" flux component in the y direction.

The EOS for the pressure is the stiffened gas law in isentropic form:

$$P = s_0 \rho^\gamma - P_\infty \quad \text{and} \quad c^2 = \frac{\gamma}{\rho}(P + P_\infty)$$

These EOS allow us to simulate perfect gas with the parameters:

$$P_\infty = 0,\ \gamma = 1.4 \text{ and } s_0 = 10^6$$

and to approach water behavior using

$$P_\infty = 10^9,\ \gamma = 2.34 \text{ and } s_0 = 95.51.$$

For gas simulation we have chosen $\rho_r = 0.5$ and $\rho_l = 1$; for water simulation we have chosen $\rho_r = 800$ and $\rho_l = 1000$. The figures (6),(7),(8) and (9) show the numerical solution computed for the gas parameters at $t = 2e^{-4}$ on the second level mesh with interface at $x_{interf} = -5h_0$ with our interface model. With these initial conditions a shock wave travels to the left upper corner of the tank, hitting the interface edges, and a rarefaction wave moves to the right lower corner of the tank (the results of figures (6),(7),(8) and (9) show the solution computed when the shock wave reaches the left upper corner).

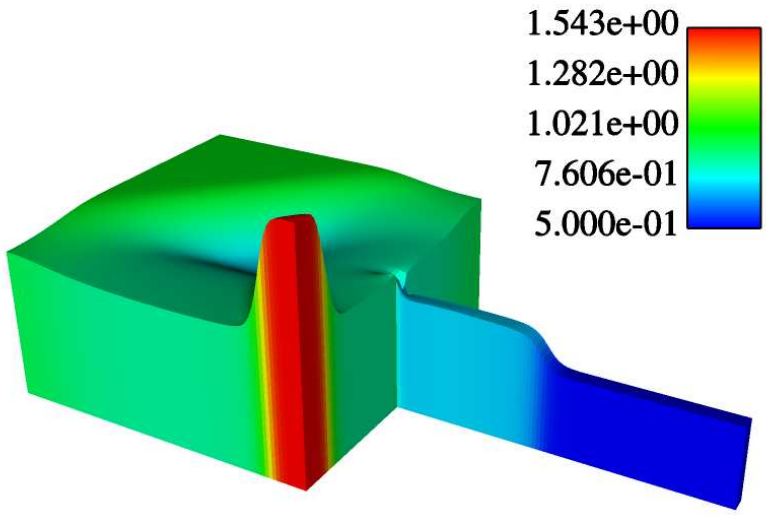

Figure 6: density map

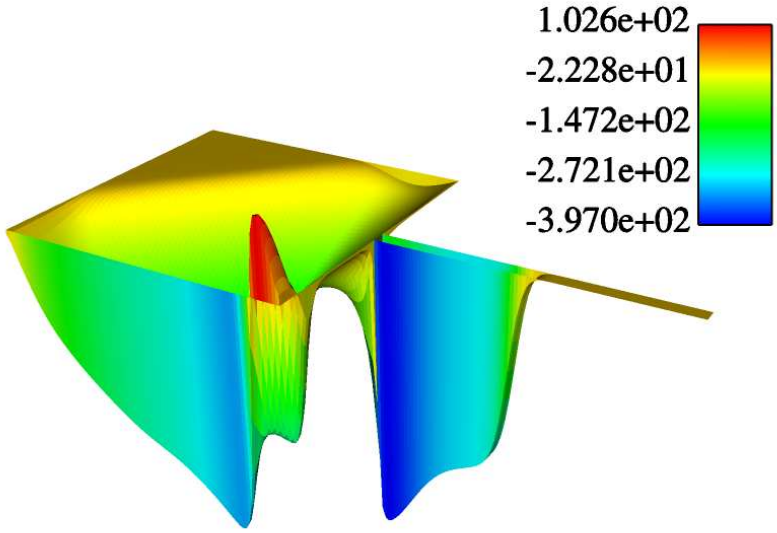

Figure 7: ρu x-momentum map

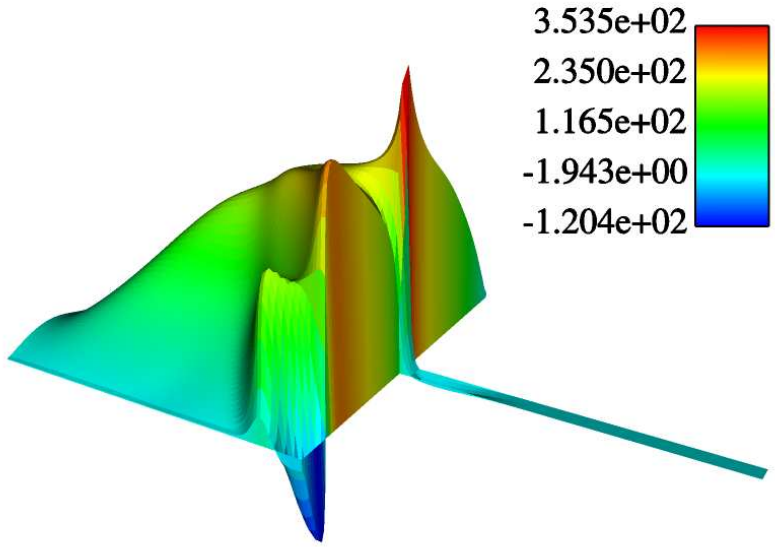

Figure 8: ρv y-momentum map

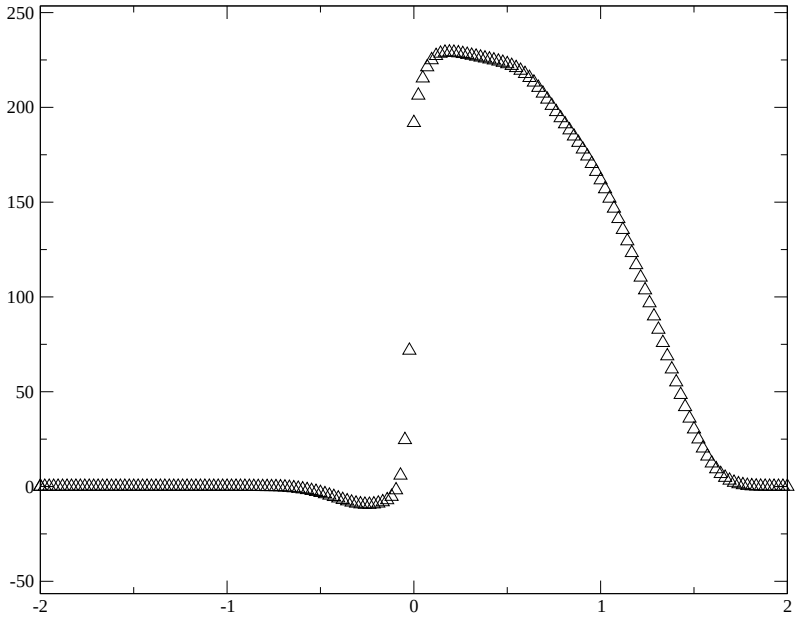

Figure 9: ρv profile along the line $y = 0$

4.3 Numerical fluxes

For both one- and two-dimensional codes we recall that we use the approximate Godunov solver VFRoe-ncv [8] to compute fluxes on each interface between two cells.

We use two different strategies to compute fluxes on both sides of the interface between the 1D code and the 2D code. We recall that (ρ^*, u^*) represent the approximate value on the interface in the solution of the linearized Riemann problem associated with (4), (5). For all schemes, numerical fluxes $(\rho^* u^*, \rho^*(u^*)^2 + P(\rho^*))$ are of course identical at the coupling interface. Thus the only discrepancies depend on the flux on the (ρv) component.

- The first strategy consists in applying the non-conservative interface model described in the section 3.3, with the VFRoe-ncv scheme, using the variable $Y^\top = (z, \rho, u, v)$. It is refered to in the following as the non-conservative model.
  - <u>if $u^* > 0$:</u>

$$(\rho uv)^- = 0$$

$$(\rho uv)^+ = 0$$

  - <u>if $u^* < 0$:</u>

$$(\rho uv)^- = 0$$

$$(\rho uv)^+ = (\rho u)^* v_R$$

- A second interface scheme is used. This scheme naturally issues from the admissible conservative model which agrees with the (NSC) described in section 3.4. Actually this scheme simply enforces the continuity on the $\rho v-$component of the flux that is:

$$(\rho uv)^+ = (\rho uv)^- = 0$$

The two other components of the flux are the same as the flux obtained with either the non-conservative model or the conservative model.

4.4 Numerical results

As a reference we compute the solution of the two-dimensional model on the whole domain with the finest mesh refinement *in the tank and in the whole pipe.*

The domain can be cut in three sudomains on which errors will be computed separately:

- the tank, $x > 0$.
- the two-dimensional part of the pipe, $0 > x > x_{interf}$ if $x_{interf} < 0$.
- the one-dimensional part of the pipe, $x_{interf} > x$.

Because of the different volumes of the different domains, we will use a normalized L_1-norm of the error e_1 at time $t^n = T$:

$$e_1(T) = \|(u - u^{ref})(T)\|_{L_1} = \frac{\sum_i |u_i^n - (u^{ref})_i^n||\Omega_i|}{\sum_i |\Omega_i|}$$

Note that $(u^{ref})_i^n$ does not stand for the exact solution, but for the approximation obtained while using the two dimensional scheme on the finest mesh on the whole computational domain, within cell i and at time t^n.

Remark. *The approximate solutions of the component ρv computed with the two interface schemes have null values for the one-dimensional pipe so that the error calculated on this domain is the L_1-norm of the solution of reference. It is obviously the same for the two schemes.*

The form of the L_1-norm of the error of the computed solution at the time T on a mesh of size h can be, in a classical manner, expressed as:

$$e_1(h, T) = C(T) \times h^\alpha$$

where the coefficient C is increasing with respect to T. The coefficient α is the rate of convergence of the scheme. We use first order schemes for which $\alpha \in [\frac{1}{2}, 1]$. Actually, when restricting to the linearly degenerated fields, we get $\alpha = \frac{1}{2}$; turning to the genuinely non-linear fields, we have: $\alpha = 1$, and thus if both fields are present in the simulation, α lies in $]\frac{1}{2}, 1[$ (see for instance [11] and [9]).

The figures below represent the $\rho v-$error with respect to $log\left(\left(\frac{h_0}{2^K}\right)^2\right)$ (with $K = \{0, 1, 2, 3\}$ the level of refinement) for the two solutions: the non-conservative model is denoted by circles and the conservative model is denoted by squares.

4.4.1 Interface $x_{interf} = 0$

We focus here on the water simulation. (Similar results have been obtained using gas EOS, associated results are given in appendix B). The interface between codes has been placed exactly at the junction between the 1D pipe and the 2D tank. The CFL is fixed to 0.95.

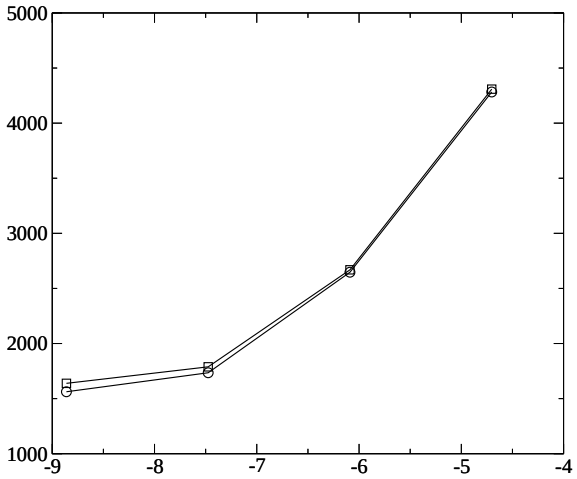

Figure 10: $\rho v-$error wrt. $log\left(\left(\frac{h_0}{2^K}\right)^2\right)$ in the 2D Tank

4.4.2 Interface $x_{interf} = -5h_0$

We use the same initial conditions, but the interface between codes is now located at $x = -5h_0$. We still use the same CFL time stepping limitation.

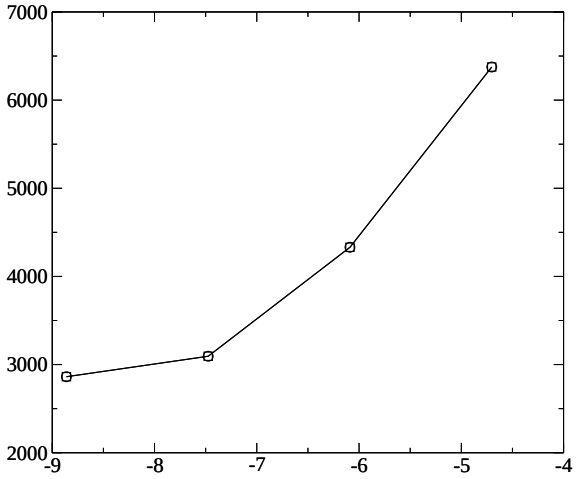

Figure 11: $\rho v-$error wrt. $log\left(\left(\frac{h_0}{2^K}\right)^2\right)$ in the 2D Tank

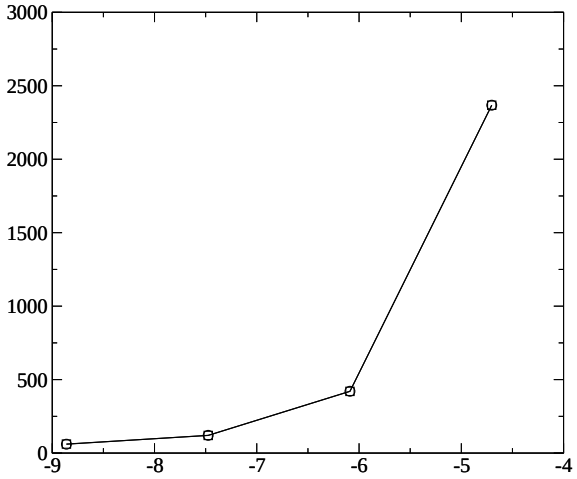

Figure 12: $\rho v-$error wrt. $log\left(\left(\frac{h_0}{2^K}\right)^2\right)$ in the 2D pipe

4.4.3 Some qualitative results in the pipe direction

We present herein the values of the field $\rho v(x, y = 0)$ (on the line $y = 0$), focusing on the finest mesh($h = h_0/8$). The squares denote the solution computed with the conservative model, the circles denote the solution for the non-conservative model and the line denotes the reference solution.

For gas simulations, it appears that the L^1 norm of the error is approximately the same for both conservative and non-conservative approaches. Nonetheless, the error is much higher close to the coupling interface when applying for the conservative model, whereas the non-conservative model results are indeed close to those provided by the reference 2D code (see figure (13)). *Actually the relative error in the cell close to the right exit of the pipe is about six times larger when using the conservative model.* This is true whereever the interface between the two codes lies (see figure (15)). We insist that this still holds true when turning to water simulations, though the discrepancies become smaller (see figures (16), (18)).

From an engineering point of view, it is almost impossible to distinguish any "spurious" reflected wave in the 2D tank.

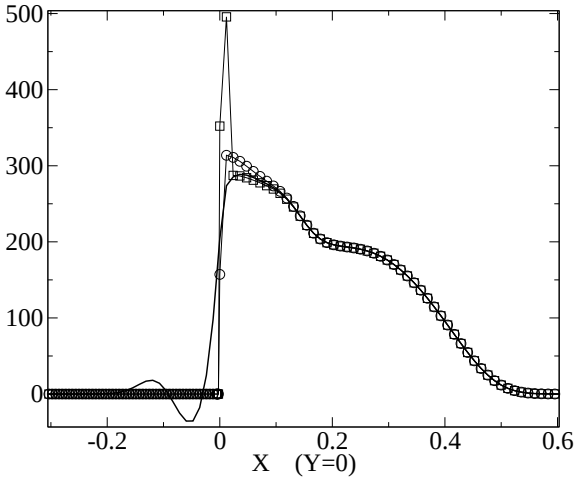

Figure 13: $\rho v(x, y = 0)$ for gas parameters and $x_{interf} = 0$

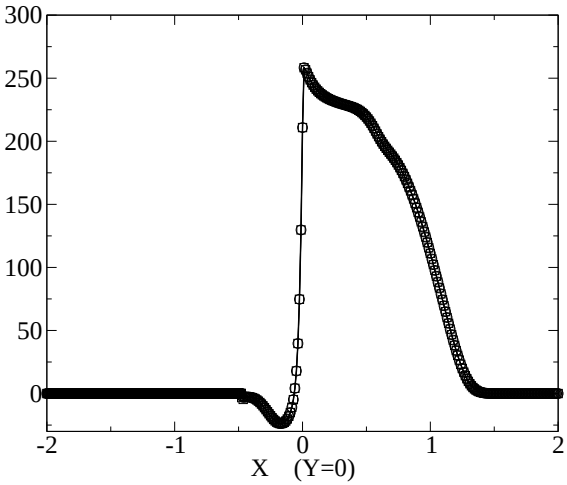

Figure 14: $\rho v(x, y = 0)$ for gas parameters and $x_{interf} = -5h_0$ (first view)

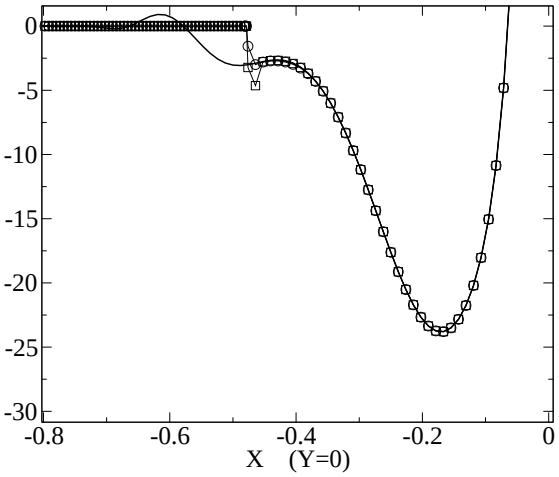

Figure 15: $\rho v(x, y = 0)$ for gas parameters and $x_{interf} = -5h_0$ (second view)

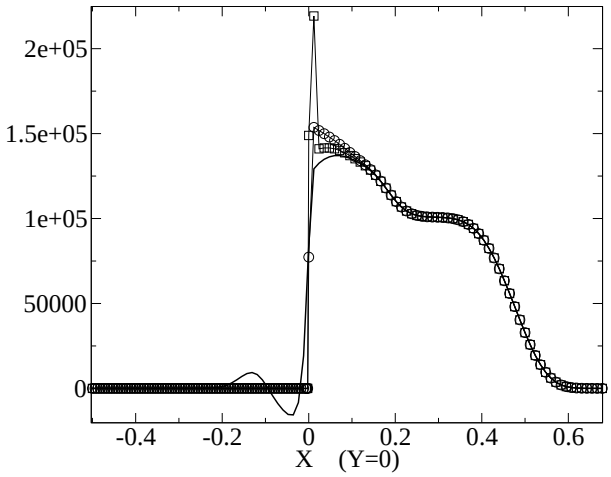

Figure 16: $\rho v(x, y = 0)$ for water parameters and $x_{interf} = 0$

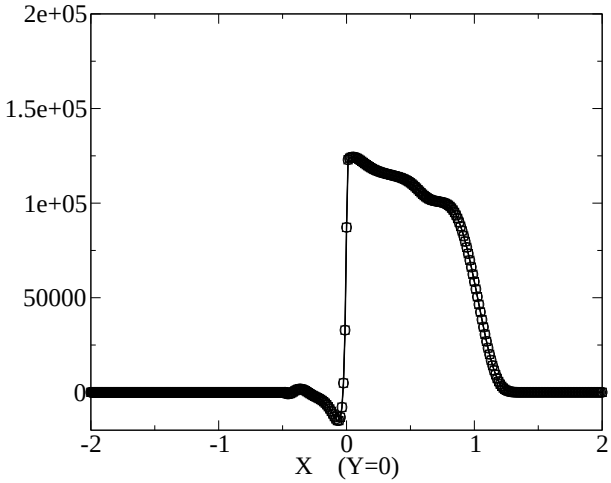

Figure 17: $\rho v(x, y = 0)$ for water parameters and $x_{interf} = -5h_0$ (first view)

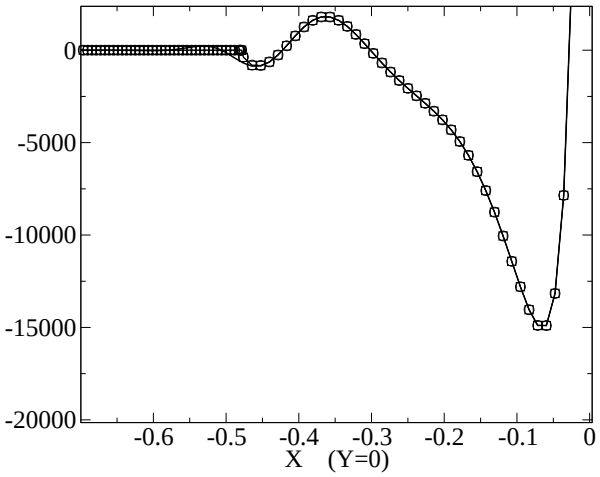

Figure 18: $\rho v(x, y = 0)$ for water parameters and $x_{interf} = -5h_0$ (second view)

4.4.4 Convergence rate

For each interface scheme, we compute two evaluations of the convergence rate. For that purpose, we use the solutions computed on the two finest meshes and on the two coarsest meshes respectively:

$$\alpha = Log(\frac{e_1(h,T)}{e_1(h/2,T)})/Log(2)$$

where the choice $h = h_0$ (respectively $h = h_0/4$) provides an approximation of α on the coarse (respectively fine) meshes. Results are given in the following tables.

Convergence rate for the interface $x_{interf} = 0$:

	Non-conservative	model	Conservative	scheme
	fine	coarse	fine	coarse
Tank 2D	0.151	0.694	0.126	0.691

Convergence rate for the interface $x_{interf} = -5h_0$:

	Non-conservative	model	Conservative	scheme
	fine	coarse	fine	coarse
Tank 2D	0.113	0.558	0.113	0.558

For the latter case $x_{interf} = -5h_0$, we note that the errors are identical, and therefore the approximations of rates of convergence. Actually, (small) discrepancies between computational results only occur in the 2D part of the pipe. This is confirmed when computing similar approximations of rates of convergence *within the part of the pipe on the right side of the coupling interface* (see below).

	Non-conservative	model	Conservative	scheme
	finest mesh	coarsest mesh	finest mesh	coarsest mesh
Pipe 2D	601.69	2367.56	612.72	2367.56

4.4.5 Comments

In the 1D part of the pipe, the approximation of v is implicitly set to 0, whereas a meaningful approximation of v arises from the part of the pipe which is simulated with a 2D code. Thus, there exists a *structural part of the global error which is due to the 1D part of the pipe*, independently of the coupling interface and its associated fluxes. This error will in any case be transmitted through the coupling interface. Thus, one expects to retrieve that the L^1 norm of the error computed in the 2D computational domain cannot tend to 0, when the mesh size tends to 0 -unless the coupling interface is moved towards the left end of the pipe-.

- *Impact of the coupling technique*
  As it has already been mentionned, the computational approximations provided by the non conservative model are in better agreement with the true 2D reference results. If one looks at the right side of the coupling interface, a glitch appears when applying for the conservative

model, and the amplitude of discrepancies will clearly inhibit the computation of chemical species which are essentially driven by the velocity field. This drawback remains almost unchanged when the mesh is refined. Such a drawback does not occur when using the non conservative model.

- *Influence of the mesh size*
  For coarse meshes, the above estimated rates of convergence α for water simulations seem to lie in $[1/2, 1]$, whereever the coupling interface lies. However, for finer meshes which necessarily provide more reliable information, the estimated rates are much lower and close to 0.1 for water simulations. If one turns to gas simulations (see appendix B), this gets worse since it appears that estimated rates of convergence are even lower, when focusing on the finer meshes for instance (the estimation of α is around 0.02). All these values thus confirm that the error in the 2D tank does not go to zero when the mesh is refined.

- *Influence of the coupling interface location*
  For a given mesh size, one may push the coupling interface to the left side. Doing so, the -meaningful- cell values of v in the 2D part of the pipe (that is on the right side of the coupling interface) naturally tend to vanish. Hence, the approximations provided by both coupling techniques can hardly be distinguished, at least when one focuses on the L^1 norm of the error in the 2D tank ; one can nonetheless note slight differences when computing the L^1 norm of the error in the 2D part of the pipe. These results are still in favour of the non conservative coupling technique, and one can retrieve this from a qualitative point of view on figure (18).

- *Influence of the EOS*
  Though we feel much more concerned by water simulations, it appears that gas simulations enable to retrieve the same patterns. The main difference is probably due to the fact that inertia effects are less important, which makes the computational results closer to those of the 2D reference solution, for a given mesh size, and a given location of the coupling interface (see the first comment above).

5 Conclusion

We thus would like to point out that :

(a) the non conservative coupling method proposed herein provides satisfactory results, at least from an engineering point of view ; the conservative coupling technique which agrees with the condition (NSC) generates a bigger pollution around the interface between codes. From an academic point of view, the main advantage of the current framework is that one can examine precisely the amount of error resulting from the "rough" approximation assumed in the 1D code;

(b) the sensitivity to the location of the interface between codes has been examined, which of course confirms *a priori* results. It urges to compute the end of the pipe connected with the 2D/3D tank with a 2D/3D code;

(c) in this particular case of the coupling of a one dimensional code with a two-dimensional code with the same "father" model, the discrete version of our non conservative interface model is similar to the one which would result from the application of ideas from [15] ;

(d) the influence of the EOS does not seem to be significant. However, estimated rates of convergence show that the remark (b) is even more crucial for water simulations ;

(e) the inclusion of finite relaxation time scales, and behind this the coupling of HEM and HRM models for instance, may be achieved using similar ideas ([20], [4], [2]). Different numerical strategies to account for these have been partially investigated in [19], which show that the problem of coupling in the steady and unsteady cases should be distinguished;

(f) a similar companion work on the full Euler equations (that is the coupling of the one-dimensional and two-dimensional Euler equations including the total energy governing equations) even confirms that the main drawback of the admissible conservative model has more annoying consequences, since the pollution around the interface may lead to a blow-up of the code, which is due to the occurence of negative discrete values of the density (see appendix C and [20]). On the other hand, the admissible non-conservative approach provides satisfactory results which are close to the reference solution.

6 Acknowledgements

This work was supported by EDF (Eléctricité de France), CEA (Commissariat à l'Energie Atomique), IRSN (Institut de Radioprotection et de Sureté Nucléaire) and FRAMATOME-ANP, in the framework of the NEPTUNE project. Computational facilities were provided by EDF. It has benefited from fruitful discussions with Annalisa Ambroso (CEA), Thierry Gallouet (Université Aix Marseille I, LATP), Christophe Chalons, Frédéric Coquel, Edwige Godlewski, Frédéric Lagoutière, Pierre-Arnaud Raviart and Nicolas Seguin (Université Paris VI, Jacques-Louis Lions laboratory). Reviewers are also acknowledged for their useful comments and suggestions.

7 Appendix A : A comparison of three distinct interface models

This appendix is devoted to the comparison of results that have been obtained when using :

(a) the natural conservative interface model which does not fulfill the (NSC) condition;

(b) the non-conservative interface model which fulfills the (NSC) condition;

(c) the conservative interface model which fulfills the (NSC) condition.

All computations have been performed using the same mesh with the finest mesh in the tank. The coupling interface is located at $x = 0$. The crosses correspond to the reference solution computed on a full 2D mesh including the pipe. Schemes associated with strategies (b) and (c) have been detailed in section 4.3. The scheme corresponding to the natural strategy (a) reads:

- $\underline{\text{if } u^* > 0 :}$ $(\rho uv)^+ = (\rho uv)^- = 0$
- $\underline{\text{if } u^* < 0 :}$ $(\rho uv)^+ = (\rho uv)^- = (\rho u)^* v_R$

We obviously check that strategies (a) and (b) provide similar results in the 2D tank, which was expected since $(\rho uv)^+$ is the same for both schemes when $u^* < 0$. Of course cell values for ρv within the pipe are non zero when using (a) whereas cell values obtained with (b) and (c) are null. The error on the first cell in the tank region is almost six times greater when using the conservative approach which fulfills the (NSC) condition, that is (c). The latter does not seem suitable, especially if one aims at computing chemical species.

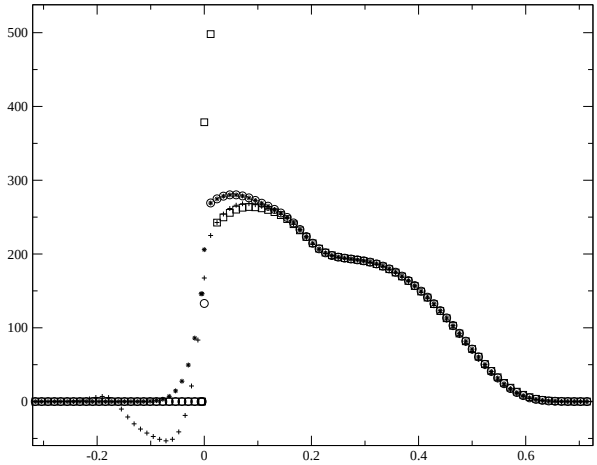

Figure 19: $\rho v(x, y = 0)$ for gas parameters and $x_{interf} = 0$. stars (a) ; circles (b) ; squares (c) ; crosses (reference 2D solution)

8 Appendix B : Error results for the gas simulation

8.0.6 Interface $x_{interf} = 0$

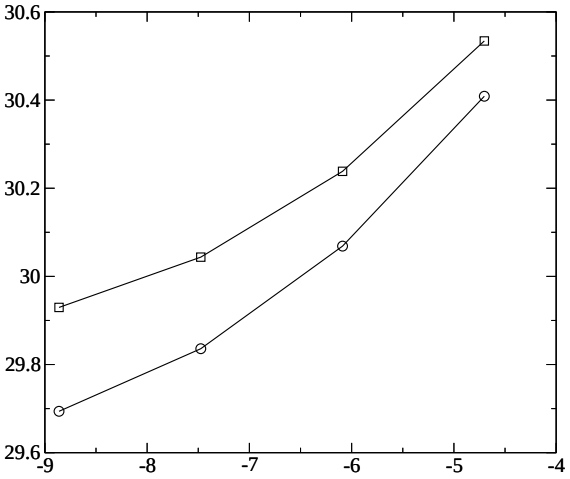

Figure 20: $\rho v-$error wrt. $log\left(\left(\frac{h_0}{2^K}\right)^2\right)$ in the 2D Tank

8.0.7 Interface $x_{interf} = -5h_0$

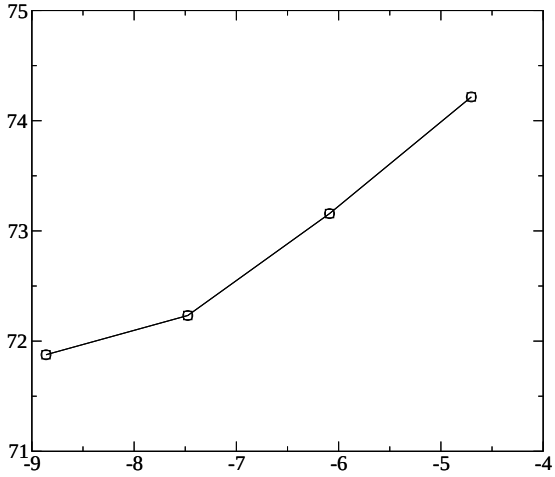

Figure 21: $\rho v-$error wrt. $log\left(\left(\frac{h_0}{2^K}\right)^2\right)$ in the 2D Tank

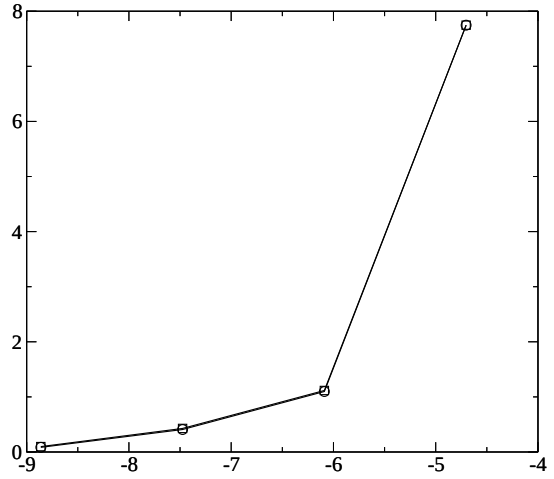

Figure 22: $\rho v-$error wrt. $log\left(\left(\frac{h_0}{2^K}\right)^2\right)$ in the 2D pipe

9 Appendix C : Coupling two and one-dimensional Euler models

In the following we explain how the methods proposed for the Euler system in isentropic form can be applied to the complete Euler system. A numerical test will reinforce the preference for the non-conservative method which respect to the (NSC).

9.1 Models to be coupled

Without loss of generality we assume that the interface of coupling is placed along the y-axis at $x = 0$. On the left side of the interface we consider the one-dimensional Euler system:

$$\frac{\partial \rho}{\partial t} + \frac{\partial (\rho u)}{\partial x} = 0 \tag{19}$$

$$\frac{\partial (\rho u)}{\partial t} + \frac{\partial (\rho u^2 + P)}{\partial x} = 0 \tag{20}$$

$$\frac{\partial E_1}{\partial t} + \frac{\partial (u(E_1 + P))}{\partial x} = 0 \tag{21}$$

with,

$$E_1 = \rho e_1(P, \rho) + \rho \frac{u^2}{2}$$

On the right side of the interface we consider the two-dimensional Euler system, the projection of which along the x-axis is (while neglecting transverse derivatives):

$$\frac{\partial \rho}{\partial t} + \frac{\partial (\rho u)}{\partial x} = 0 \tag{22}$$

$$\frac{\partial (\rho u)}{\partial t} + \frac{\partial (\rho u^2 + P)}{\partial x} = 0 \tag{23}$$

$$\frac{\partial E_2}{\partial t} + \frac{\partial (u(E_2 + P))}{\partial x} = 0 \tag{24}$$

$$\frac{\partial (\rho v)}{\partial t} + \frac{\partial (\rho u v)}{\partial x} = 0 \tag{25}$$

with,

$$E_2 = \rho e_2(P, \rho) + \rho(\frac{u^2}{2} + \frac{v^2}{2})$$

In the following we will consider that the two models have the same equation of state, that is :

$$e_1(P, \rho) = e_2(P, \rho) = e(P, \rho), \quad \forall (P, \rho)$$

9.2 Rewriting the two-dimensional Euler system

We note that the total energy E_2 can be expressed as:

$$E_2 = E_1 + \rho \frac{v^2}{2}$$

The set of equations (22)-(25) is equivalent to the set of equations (26)-(29), either for regular solutions or for discontinuities:

$$\frac{\partial \rho}{\partial t} + \frac{\partial (\rho u)}{\partial x} = 0 \tag{26}$$

$$\frac{\partial (\rho u)}{\partial t} + \frac{\partial (\rho u^2 + P)}{\partial x} = 0 \tag{27}$$

$$\frac{\partial E_1}{\partial t} + \frac{\partial (u(E_1 + P))}{\partial x} = 0 \tag{28}$$

$$\frac{\partial (\rho v)}{\partial t} + \frac{\partial (\rho u v)}{\partial x} = 0 \tag{29}$$

An important point to be quoted is that the subset of equations (26)-(28) does not depend on v. It is the same set of equations than (19)-(21). We can then apply the methods of flux coupling proposed for the isentropic Euler model.

9.3 An interface model for flux coupling

The (NSC) condition keeps its importance in the present case. Hence an interface model is admissible if and only if it respects this condition. We propose herein two models. The definition of the variable z remains unchanged.

9.3.1 A non-conservative admissible interface model

We now consider the following interface model:

$$\frac{\partial z}{\partial t} = 0 \tag{30}$$

$$\frac{\partial \rho}{\partial t} + \frac{\partial (\rho u)}{\partial x} = 0 \tag{31}$$

$$\frac{\partial (\rho u)}{\partial t} + \frac{\partial (\rho u^2 + P)}{\partial x} = 0 \tag{32}$$

$$\frac{\partial E_1}{\partial t} + \frac{\partial (u(E_1 + P))}{\partial x} = 0 \tag{33}$$

$$\frac{\partial v}{\partial t} + zu\frac{\partial v}{\partial x} = 0 \tag{34}$$

This system can not be written in conservative form owing to the non-conservative product $zu\dfrac{\partial v}{\partial x}$. In fact the solution of the Riemann problem is classical for (30)-(33) (unless some resonance phenomena occurs), but we have to propose a way to solve (34). This is achieved using the same idea as developed in the isentropic case. Finally, the numerical fluxes are:

$$F^- = \begin{pmatrix} (\rho u)^* \\ (\rho u^2 + P)^* \\ (u(E_1 + P))^* \\ 0 \end{pmatrix} \quad , \quad F^+ = F^- + \begin{pmatrix} 0 \\ 0 \\ \frac{(\rho u)^*}{2}(v^+)^2 \\ (\rho u)^* v^+ \end{pmatrix}$$

where v^+ is the solution for the variable v at $x/t = 0^+$ and Y^* stands for the exact solution $Y(x/t = 0)$. Obviously the coupling method respects the (NSC) condition and is not conservative.

9.3.2 A conservative admissible interface model

We introduce now a conservative interface model that respects the (NSC) condition. This model is exactly the counterpart of the conservative model proposed for the isentropic case. The governing equations are:

$$\frac{\partial z}{\partial t} = 0 \tag{35}$$

$$\frac{\partial \rho}{\partial t} + \frac{\partial (\rho u)}{\partial x} = 0 \tag{36}$$

$$\frac{\partial (\rho u)}{\partial t} + \frac{\partial (\rho u^2 + P)}{\partial x} = 0 \tag{37}$$

$$\frac{\partial E_1}{\partial t} + \frac{\partial (u(E_1 + P))}{\partial x} = 0 \tag{38}$$

$$\frac{\partial (\rho v)}{\partial t} + \frac{\partial (zu\rho v)}{\partial x} = 0 \tag{39}$$

Hence the left and right fluxes are:

$$F^- = F^+ = \begin{pmatrix} (\rho u)^* \\ (\rho u^2 + P)^* \\ (u(E_1 + P))^* \\ 0 \end{pmatrix}$$

Thus this model fulfils the (NSC) condition and since $F^- = F^+$ this coupling method is also conservative in terms of total energy.

9.4 Numerical results

We use the above methods to simulate the Euler model with perfect gas EOS, that is:

$$(\gamma - 1)\rho e(P, \rho) = P$$

The test case configuration is the same as the one described for the isentropic Euler systems. We choose to present the results obtained for the gas simulation, that is $\gamma = 1.4$. The initial conditions are:

$$\rho(x, y; t = 0) = \begin{cases} 0.5 & \text{if } \ y > x - 0.15 \\ 1.0 & \text{else.} \end{cases}$$

$$P(x, y; t = 0) = \begin{cases} 10^4 & \text{if } \ y > x - 0.15 \\ 10^5 & \text{else.} \end{cases}$$

$$u(x, y; t = 0) = v(x, y; t = 0) = 0.0$$

The interface is located in $x = 0$ (i.e. at the connection between the pipe and the tank). All interfacial fluxes are computed using a VFRoe-ncv scheme with the variable $(\rho, u, P, v)^\top$ and the time steps are computed in order to comply with the constraint: $CFL = 1/2$.

The density ρ and the transverse momentum ρv are plotted on the line $y = 0$ (with respect to x). The so-called two-dimensional reference solution is the computation obtained using the

two-dimensional Euler model on the whole domain with the mesh refined in all directions. The results which are displayed result from the finest mesh. For the conservative admissible model the overshoot of the transverse velocity makes the computation stop (the density in at least one cell becomes negative). Results are plotted at the last time step before this blow-up occurs.

Moreover, when compared with the conservative admissible model (represented by squares on figures), we observe that results obtained with the non-conservative admissible model (represented by circles on figures) are much closer to the $2D$ reference solution (represented by crosses on figure) near the coupling interface.

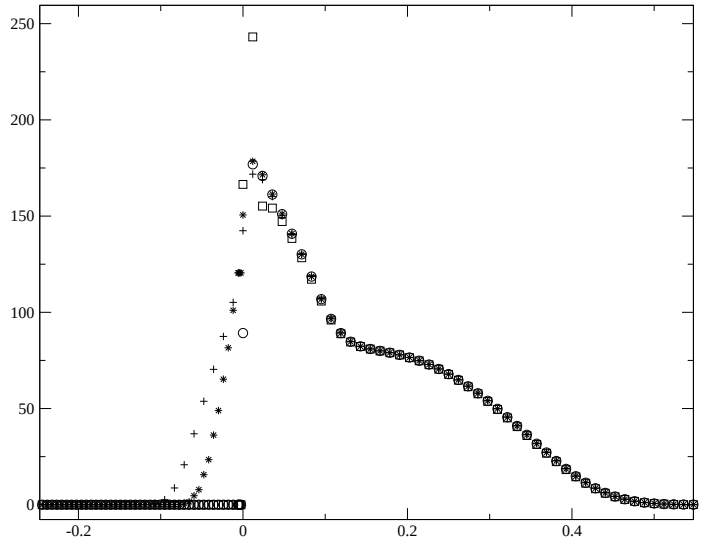

Figure 23: Solution for the transverse momentum ρv on the line y=0. Crosses stand for the two-dimensional reference solution, stars stand for the natural interface model (which does not respect the (NSC)), circles stand for the non conservative admissible interface model and squares stand for the conservative admissible interface model.

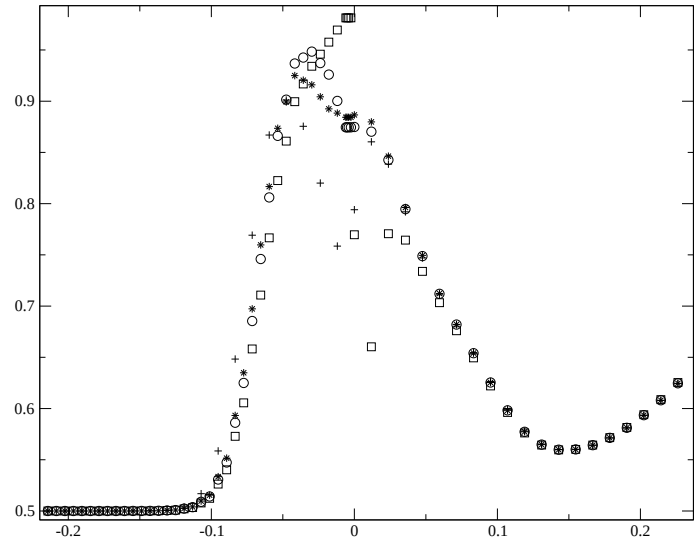

Figure 24: Solution for the density on the line y=0. Crosses stand for the two-dimensional reference solution, stars stand for the natural interface model (which does not respect the (NSC)), circles stand for the non conservative admissible interface model and squares stand for the conservative admissible interface model.

References

[1] R. Abgrall and S. Karni, Computation of compressible multifluids, *J. Comp. Phys.*, 2001, vol. 169, pp. 594–623.

[2] A. Ambroso, C. Chalons, F. Coquel, E. Godlewski, F. Lagoutiere, P.A. Raviart and N. Seguin, Coupling of homogeneous models for two-phase flows, *in preparation.*

[3] ——, Coupling of multiphase flow models, *in NURETH 11 proceedings, Avignon, France*, 2-6 october, 2005.

[4] ——, Homogeneous models with phase transition: coupling by finite volume methods, *in FVCA4 proceedings, Penton Hermes Science, Marroco*, july 4-8, 2005.

[5] A. Ambroso, C. Chalons, F. Coquel, E. Godlewski and P.A. Raviart, Couplage de deux systèmes de la dynamique des gaz, *Congrès Francais de Mécanique, Troyes, France*, august 29-september 2, 2005.

[6] F. Bachmann, Analysis of a scalar conservation law with a flux function with discontinuous coefficients, *Advances in Differential Equations*, 2004, vol. 11-12, pp. 1317–1338.

[7] F. Bachmann and J. Vovelle, Existence and uniqueness of entropy solution of scalar conservation law with a flux function involving discontinuous coefficients, *Communications in Partial Differential Equations*, to appear.

[8] T. Buffard, T. Gallouët and J.M. Hérard, A sequel to a rough Godunov scheme. Application to real gases, *Computers and Fluids*, 2000, vol. 29-7, pp. 813–847.

[9] R. Eymard, T. Gallouët and R. Herbin, Finite Volume Methods, In *Handbook of Numerical Analysis* (Vol. VII), editors : P.G. Ciarlet and J.L. Lions, pp. 729–1020, North-Holland, 2000.

[10] Y. Fournier, Calculation of local flow conditions in the lower core of a pwr with code saturne, *Supercomputing for Nuclear Applications*, 2003.

[11] T. Gallouët, J.M. Hérard and N. Seguin, Some recent Finite Volume schemes to compute Euler equations using real gas EOS, *Int. J. for Num. Meth. in Fluids*, 2002, vol. 39, pp. 1073–1138.

[12] ——, Some approximate Godunov schemes to compute shallow water equations with topography, *Computers and Fluids*, 2003, vol. 32, pp. 479–513.

[13] E. Godlewski and P. A. Raviart, The numerical interface coupling of nonlinear hyperbolic systems of conservation laws: 1.the scalar case, *Numerische Mathematik*, 2004, vol. 97, pp. 81–130.

[14] E. Godlewski and P.A. Raviart, *Numerical analysis for hyperbolic systems of conservation laws*, Springer Verlag, 1996.

[15] E. Godlewski, K. C. Le Thanh and P. A. Raviart, The numerical interface coupling of nonlinear hyperbolic systems of conservation laws: 2.the case of systems, *Math. Mod. Num. Anal.*, 2005, vol. 39, pp. 649–692.

[16] S.K. Godunov, A difference method for numerical calculation of discontinous equations of hydrodynamics, *Sbornik*, 1959, pp. 271–300. In Russian.

[17] J.M. Greenberg and A.Y. Le Roux, A well balanced scheme for the numerical processing of source terms in hyperbolic equation, *SIAM J. Numer. Anal.*, 1996, vol. 33-1, pp. 1–16.

[18] J.M. Hérard, Naive schemes to compute isentropic flows between free and porous medium, *internal EDF report HI81/04/008/A, also in AIAA paper 2005-4861*, 2004.

[19] J.M. Hérard and O. Hurisse, A few schemes to compute hyperbolic systems with source terms, *EDF report HI81/04/007/A, also in AIAA paper 2005-4988*, 2004.

[20] O. Hurisse, PhD thesis, Université Aix Marseille I, France, In preparation.

[21] J.U. Schluter, Consistent boundary conditions for integrated rans/les simulations: Les inflow conditions, *AIAA paper 2003-3971, see also http://www.stanford.edu/group/cits*, 2003.

[22] J.U. Schluter, H. Pitsch and P. Moin, Consistent boundary conditions for integrated rans/les simulations: Les outflow conditions, *AIAA paper 2002-3121, see also http://www.stanford.edu/group/cits*, 2002.

[23] J.U. Schluter, X. Wu, E. van der Weide, S. Hahn, J. Alonso and H. Pitsch, Multi-code simulations: a generalized coupling approach, *AIAA paper 2005-4997, see also http://www.stanford.edu/group/cits*, 2005.

[24] N. Seguin and J. Vovelle, Analysis and approximation of a scalar conservation law with a flux function with discontinuous coefficients, *Math. Mod. and Methods in Applied Sciences*, 2003, vol. 13-2, pp. 221–257.

[25] J. Smoller, *Shock waves and reaction diffusion equations*, Springer Verlag, 1983.